

Cosmic Ray Rejection by Linear Filtering of Single Images¹

James E. Rhoads

Kitt Peak National Observatory, 950 North Cherry Avenue, Tucson, AZ 85719²;
jrhoads@noao.edu

ABSTRACT

We present a convolution-based algorithm for finding cosmic rays in single well-sampled astronomical images. The spatial filter used is the point spread function (approximated by a Gaussian) minus a scaled delta function, and cosmic rays are identified by thresholding the filtered image. This filter searches for features with significant power at spatial frequencies too high for legitimate objects. Noise properties of the filtered image are readily calculated, which allows us to compute the probability of rejecting a pixel not contaminated by a cosmic ray (the false alarm probability). We demonstrate that the false alarm probability for a pixel containing object flux will never exceed the corresponding probability for a blank sky pixel, provided we choose the convolution kernel appropriately. This allows confident rejection of cosmic rays superposed on real objects. Identification of multiple-pixel cosmic ray hits can be enhanced by running the algorithm iteratively, replacing flagged pixels with the background level at each iteration.

Subject headings: techniques: image processing

1. Introduction

Images from most current-day astronomical instruments have tractable noise properties. An exemplary case is optical images from CCD detectors, whose uncertainties are generally dominated by the Poisson statistics of the detected photons, with (usually smaller) contributions from detector read noise, dark current, and other comparatively minor nuisances. Most of these noise sources are well approximated by Gaussian distributions, and their sum is therefore also well approximated by a Gaussian.

Cosmic rays impinging on a detector can yield large signals over single pixels or small groups of pixels, thereby introducing a distinctly non-Gaussian tail to the noise distribution. The most

¹ Accepted for publication in the May 2000 issue of the *Publications of the Astronomical Society of the Pacific*.

²Current address: Space Telescope Science Institute, 3700 San Martin Drive, Baltimore, MD 21218; rhoads@stsci.edu

common approach to removing cosmic rays from astronomical images is to take multiple exposures and combine them with some sort of outlier rejection. Real astronomical objects should (usually) be present on multiple frames, while cosmic ray hits will not generally repeat. Such methods have been presented in the literature by (e.g.) Shaw & Horne (1992) and Windhorst, Franklin, & Neuschaefer (1994), and are widely implemented in astronomical image processing packages.

However, there are times when multiple images are not available, or when the sources of interest may be moving or varying on timescales short compared to the interval between exposures. In these cases, a cosmic ray rejection method capable of operating on single exposures is necessary. Cosmic ray rejection in single frames can also be useful even when multiple exposures are to be stacked, since stacking often requires spatial interpolation of the input images, and any cosmic rays not previously identified can be spread over many pixels by spatially extended interpolation kernels. Additionally, if a stack of images has widely different point spread function (PSF) widths, rejection algorithms used while stacking tend either to be overly lenient, potentially admitting cosmic rays; or overly strict, discarding valid data from images with very good or very bad seeing. Examples of both these behaviors are offered by sigma clipping algorithms, where the contribution of a particular exposure to a stack is discarded if it differs from the mean (or median) intensity at that location by more than $k\sigma$, where k is a constant (generally with $2 \lesssim k \lesssim 5$) and σ measures the intensity uncertainty at that location. If σ is measured directly from the list of exposure intensities at a fixed sky position, a lenient rejection results, while if σ is taken from the known Poisson statistics of electrons in single exposures, a strict rejection results.

To identify cosmic rays in single exposures, rejection algorithms rely on the sharpness of cosmic rays relative to true astronomical objects. That is, any legitimate object in our astronomical image is blurred by the PSF, but there is no such requirement on cosmic ray hits. Provided the image is well-sampled (in practice, $\gtrsim 2$ pixels across the PSF full width at half maximum), cosmic ray hits can be identified as those features with spatial variations too rapid for consistency with the PSF. Murtagh (1992) and Salzberg et al (1995) have explored trainable classifier approaches to single-image cosmic ray rejection. Their methods have the advantage of applicability to substantially undersampled data (from the WF/PC-I instrument on the Hubble Space Telescope). On the other hand, these methods ultimately rely on a training set, which may be subjectively defined.

The present paper explores a method suggested by Fischer and Kochanski (1994), who remark that the optimal filter for detecting [single-pixel] cosmic ray hits is the point spread function minus a delta function. This can be regarded as a difference between the matched filter for detecting point sources (i.e. the PSF) and that for detecting single pixels (i.e. a delta function). There is one free parameter in such a filter, which is the amplitude ratio of the two functions. We develop this filtering method in detail by considering the cosmic ray rejection rates and false alarm rates. Much of our analysis is devoted to choosing the delta function amplitude appropriately. With a careful choice of this parameter, it is possible to ensure that the false alarm rate nowhere exceeds its value in blank sky regions.

In section 2, we derive the noise properties of our filtered image, and explain how to tune the filter to avoid excessive rejection of valid data. In section 3, we discuss practical issues that arise when implementing our algorithm. Section 4 presents simulations used to verify the algorithm’s performance. Finally, in section 5 we summarize our work, describe our usual application for our algorithm, and comment on a desirable future direction for cosmic ray rejection algorithms.

2. Mathematical formalism

Suppose we have an image I with the following properties: First, it has some background level B_I and noise σ_I , and the sky noise is uncorrelated between any pair of pixels. Second, it is linear in the input signal with a gain g photons per count, so that a pixel containing object flux S counts will have a noise contribution of $\sqrt{S/g}$ counts from Poisson noise in the object signal. Third, it has a point spread function that can be well approximated by a Gaussian of characteristic width ξ (i.e., the stellar profiles have a functional form $\propto \exp[-(\Delta x^2 + \Delta y^2)/(2\xi^2)]$), and is well sampled (i.e., $\xi \gtrsim 1$ pixel). This third property is an analytical convenience that is reasonably near truth for seeing-limited optical images from ground-based telescopes. Other PSF models would complicate the mathematical analysis that follows, but would not greatly change either its flavor or its quantitative results.

Now consider convolving this image with a spatial filter F consisting of a unit-normalized point spread function $A = \exp[-(\Delta x^2 + \Delta y^2)/(2\xi^2)]/(2\pi\xi^2)$ minus a scaled delta function: $F = A - \alpha\delta(\Delta x)\delta(\Delta y)$. Call the convolved image J , so that $J = I * F = I * A - \alpha I$. (Here and throughout the paper, “ $*$ ” is the convolution operator.)

If we regard the convolution kernel as a matched filter, it is clear that a broader kernel (likely using a functional form besides the Gaussian) would be more effective at separating cosmic rays from faint galaxies or other extended sources. However, almost all astronomical images contain some legitimate pointlike sources, which should not be rejected. Using a template more extended than a point source would risk rejecting stars, and such templates are therefore not explored further.

2.1. Noise properties of the filtered image

We calculate the noise in the convolved image in two steps, first determining the noise in $I * A$ and then modifying the result to account for the second term in filter F . Treating the noise in each pixel as an independent random variable with variance σ_I^2 , the variance in the convolved image is simply a weighted sum $\sigma_J^2 = \sum_{\ell} w_{\ell}^2 \sigma_{I,\ell}^2$, where the sum runs over pixels and w_{ℓ} is simply F evaluated at the location $(\Delta x_{\ell}, \Delta y_{\ell})$ of pixel ℓ . Now, in regions of blank sky, $\sigma_{I,\ell} \equiv \sigma_I$ is constant, so $\sigma_{I*F} = \sigma_I^2 \sum_{\ell} w_{\ell}^2$.

We can calculate the noise level in $I * A$ by defining weights v_ℓ as A evaluated at $(\Delta x_\ell, \Delta y_\ell)$, and noting that

$$\frac{\sigma_{I*A}^2}{\sigma_I^2} = \sum_\ell v_\ell^2 \approx \int_0^\infty \frac{2\pi r dr}{(2\pi\xi^2)^2} \left[\exp\left(\frac{-r^2}{2\xi^2}\right) \right]^2 = \frac{1}{4\pi\xi^2} , \quad (1)$$

so that $\sigma_{I*A}^2 = \sigma_I^2/(4\pi\xi^2)$. The continuous approximation to the discrete sum made here should be reasonably accurate for well-sampled data.

Modifying this for the central pixel, which has weight $w = 1/(2\pi\xi^2) - \alpha$ rather than $v = 1/(2\pi\xi^2)$ as used above, we find

$$\frac{\sigma_J^2}{\sigma_I^2} = \sum_\ell w_\ell^2 \approx \frac{1}{4\pi\xi^2} - \left(\frac{1}{2\pi\xi^2}\right)^2 + \left(\frac{1}{2\pi\xi^2} - \alpha\right)^2 = \frac{1}{4\pi\xi^2} - \frac{\alpha}{\pi\xi^2} + \alpha^2 . \quad (2)$$

That accomplished, we can determine the significance level that a cosmic ray with amplitude $n\sigma_I$ will have in image J . A single pixel cosmic ray with C_I counts will result in a pixel with expectation value $C_J = [1/(2\pi\xi^2) - \alpha] C_I$ below the sky level of J (which is $B_J = (1 - \alpha)B_I$). If $C_I = n\sigma_I$, then the final significance level is

$$\frac{-C_J}{\sigma_J} = \frac{C_I}{\sigma_I} \times \frac{1/(2\pi\xi^2) - \alpha}{(1/(4\pi\xi^2) - \alpha/(\pi\xi^2) + \alpha^2)^{1/2}} = \frac{C_I}{\sigma_I} \times \left[1 + \frac{\pi\xi^2 - 1}{(2\pi\xi^2\alpha - 1)^2} \right]^{-1/2} . \quad (3)$$

In general, this is a lower significance level than in the original image. In the limit of very well sampled data ($\xi \rightarrow \infty$) this reduces to a significance level of C_I/σ_I , recovering the input as one might expect. The gradual approach to this limit simply reflects the dependence of cosmic ray identification on the sampling of an image. Figure 1 shows contours of $-C_J\sigma_I/(C_I\sigma_J)$.

When we reject cosmic rays, we need to be careful not to reject the cores of legitimate point sources. In order to avoid doing so, we calculate the noise level at a location near a point source, making the same continuous approximation to discrete sums used in deriving equation 1. The complication arising in this procedure is that the presence of a source changes the noise properties of the image. A pixel containing object flux I_ℓ has noise level given by $\sigma_{I,\ell}^2 = \sigma_I^2 + I_\ell/g$.

We consider below the noise at a location q pixels from the location of a star with peak counts S_0 , and define function $S_I(q) = S_0 \exp[-q^2/(2\xi^2)]$. In the convolved image, this pixel has expected flux

$$S_J(q) = S_0 \left(\frac{1}{2} \exp\left[\frac{-q^2}{4\xi^2}\right] - \alpha \exp\left[\frac{-q^2}{2\xi^2}\right] \right) . \quad (4)$$

Since variances add linearly, modifying our earlier analysis for the additional noise term is relatively straightforward. For image $I * A$, we find

$$\sigma_{A*I}^2(q) = \sum_\ell v_\ell^2 \sigma_{I,\ell}^2 \quad (5)$$

$$= \sum_{\Delta x} \sum_{\Delta y} \left(\frac{1}{2\pi\xi^2} \exp\left[\frac{-(\Delta x^2 + \Delta y^2)}{2\xi^2}\right] \right)^2 \left(\sigma_I^2 + \frac{S_0}{g} \exp\left[\frac{-([\Delta x - q]^2 + \Delta y^2)}{2\xi^2}\right] \right) \quad (6)$$

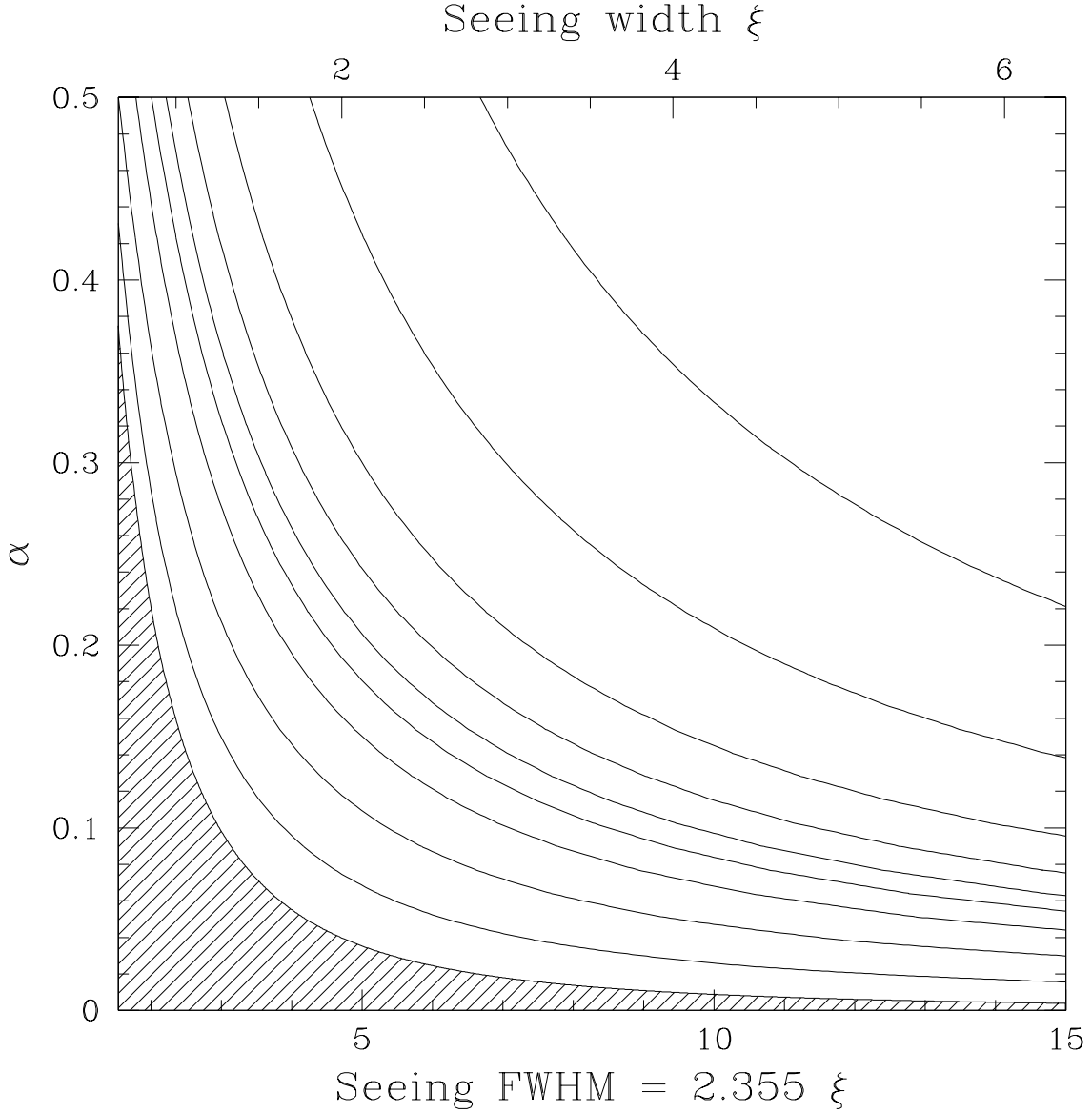


Fig. 1.— Contours show the factor $-C_J \sigma_I / (C_I \sigma_J)$ by which a single-pixel cosmic ray's significance is reduced in the convolved image J , as a function of the seeing and the scale factor α for the delta function in the convolution kernel. Contour levels are 0.98, 0.95, 0.90, 0.85, 0.80, 0.75, 0.667, 0.50, 0.25, and 0, beginning with the top right corner and continuing to the boundary of the hatched region. The crosshatching indicates the region of the parameter space where $\alpha < 1/(2\pi\xi^2)$, where the method will necessarily fail.

where we have assumed (without loss of generality) that the offset to the star is along the x -axis. Defining $\Delta x' = \Delta x - q/3$, and substituting our result from equation 1, this becomes

$$\sigma_{A*I}^2(q) = \frac{\sigma_I^2}{4\pi\xi^2} + \frac{S_0}{(2\pi\xi^2)^2 g} \exp\left[\frac{-q^2}{3\xi^2}\right] \sum_{\Delta x} \sum_{\Delta y} \exp\left[\frac{-3(\Delta x'^2 + \Delta y^2)}{2\xi^2}\right] \quad (7)$$

$$\approx \frac{\sigma_I^2}{4\pi\xi^2} + \frac{S_0}{(2\pi\xi^2)^2 g} \exp\left[\frac{-q^2}{3\xi^2}\right] \int_0^\infty 2\pi r \exp\left[\frac{-3r^2}{2\xi^2}\right] dr \quad (8)$$

$$= \frac{\sigma_I^2}{4\pi\xi^2} + \exp\left[\frac{-q^2}{3\xi^2}\right] \frac{S_0/g}{6\pi\xi^2} . \quad (9)$$

Again modifying the result to account for the delta function in the convolution kernel, we obtain for the noise at distance q from the point source

$$\sigma_J^2(q) = \sigma_{A*I}^2 + (\sigma_I^2 + S_I(q)/g) \left(\left[\frac{1}{2\pi\xi^2} - \alpha \right]^2 - \left[\frac{1}{2\pi\xi^2} \right]^2 \right) \quad (10)$$

$$= \sigma_I^2 \left(\frac{1}{4\pi\xi^2} - \frac{\alpha}{\pi\xi^2} + \alpha^2 \right) + \frac{S_0}{g} \exp\left[\frac{-q^2}{2\xi^2}\right] \left(\frac{\exp[+q^2/(6\xi^2)]}{6\pi\xi^2} - \frac{\alpha}{\pi\xi^2} + \alpha^2 \right) . \quad (11)$$

In the limit $q \rightarrow \infty$, this expression reproduces our blank sky result (equation 2), while at the peak of the star, it simplifies somewhat as the exponential terms go to unity.

These results can easily be generalized to a superposition of point sources; the second terms on the right hand sides of equations 4 and 11 would simply be replaced by a sum of such terms, each with its own value of the intensity parameter S_0 and distance parameter q .

2.2. Keeping the valid peaks

To identify cosmic rays in our image, we plan to threshold the convolved image J , flagging all pixels with excessively negative values in J . There are two probabilities of interest here, namely the probability that we will correctly flag a cosmic ray with intensity C_I (the detection rate), and the probability that we will incorrectly flag a pixel without cosmic ray flux (the false alarm rate). We have chosen to concentrate our efforts on controlling the false alarm rate, and to accept the resulting detection rate. From a hypothesis testing perspective (e.g., Kendall & Stuart 1967, chapter 22), this approach corresponds to making the null hypothesis that a given pixel is uncontaminated by cosmic ray flux. The false alarm rate is then the probability of a type I error. Missed cosmic ray events are type II errors, and their probability can be calculated as a function of cosmic ray intensity. The tradeoffs between these two errors for a variety of cosmic ray rejection algorithms are reviewed by Murtagh & Adorf (1991).

We can never set the probability of rejecting valid pixels to be precisely zero so long as we have noise in our image and we reject any pixels at all. Instead we note that there is some

finite probability p_{sky} of rejecting an arbitrary sky pixel, and demand that the probability p_{obj} of rejecting a pixel containing positive object flux not exceed p_{sky} .

Consider a threshold level in image J , $t = -k\sigma_J$. The expected count level in J is given by equation 4, and the noise level there is given by equation 11. We demand that

$$S_J(q) - k\sigma_J(q) \geq -k\sigma_J(\infty) \quad (12)$$

in order to ensure that $p_{obj} \leq p_{sky}$. By using our previous expressions for $S_J(q)$ and $\sigma_J(q)$, we convert this into a constraint on α . An immediate (though weak) constraint is that $0 \leq \alpha < 1/2$, since $\sigma_J(0) > \sigma_J(\infty)$, and the expected count rate must be positive to compensate for the increased noise at the star's location.

In the remainder of section 2, we derive conditions guaranteeing that inequality 12 will hold for all values of S_0 and q . Readers who are not interested in the mathematical details may wish to skim section 2.3, which explains how to choose the parameter α , and then move on to section 3, where we discuss implementation of the cosmic ray rejection algorithm.

By construction, condition 12 is fulfilled as an equality for $S_0 = 0$ and for any value of q . To ensure that 12 holds for all $S_0 > 0$, it is sufficient to show that

$$\frac{d}{dS_0} [S_J(q) - k\sigma_J(q)] \geq 0 \quad (13)$$

for all $S_0 > 0$ and for arbitrary q . Multiplying relation 13 by $\exp[+q^2/(4\xi^2)]$, substituting previous results for $S_J(q)$ and for $\sigma_J(q)$, and using $d\sigma_J(q)^2/dS_0 = 2\sigma_J(q) \times d\sigma_J(q)/dS_0$, we obtain

$$\begin{aligned} \mathcal{L} = & \left(\frac{1}{2} - \alpha \exp \left[\frac{-q^2}{4\xi^2} \right] \right) - \frac{k}{2g} \exp \left[\frac{-q^2}{4\xi^2} \right] \left\{ \frac{\exp [+q^2/6\xi^2]}{6\pi\xi^2} - \frac{\alpha}{\pi\xi^2} + \alpha^2 \right\} / \\ & \left\{ \sigma_I^2 \left[\frac{1}{4\pi\xi^2} - \frac{\alpha}{\pi\xi^2} + \alpha^2 \right] + \frac{S_0}{g} \exp \left[\frac{-q^2}{2\xi^2} \right] \left[\frac{\exp [+q^2/6\xi^2]}{6\pi\xi^2} - \frac{\alpha}{\pi\xi^2} + \alpha^2 \right] \right\}^{1/2} \geq 0 \end{aligned} \quad (14)$$

for all $S_0 > 0$.

We now assert that for well-behaved images, it is possible to choose α so that relation 14 is fulfilled as an equality for $S_0 = 0$ and $q = 0$. We will justify this assertion in section 2.3 below.

Taking as a hypothesis for now that $\mathcal{L} = 0$ for $S_0 = 0$ and $q = 0$, we first examine the case $S_0 = 0$, $q > 0$. Substituting $S_0 = 0$ in equation 14 and rearranging,

$$\begin{aligned} 1/2 \geq & \exp \left[\frac{-q^2}{4\xi^2} \right] \left\{ \alpha + \frac{k}{2g\sigma_I} \left(\alpha^2 - \frac{\alpha}{\pi\xi^2} \right) / \sqrt{\frac{1}{4\pi\xi^2} - \frac{\alpha}{\pi\xi^2} + \alpha^2} \right\} \\ & + \exp \left[\frac{-q^2}{12\xi^2} \right] k / \left\{ 12\pi g\sigma_I \xi^2 \sqrt{\frac{1}{4\pi\xi^2} - \frac{\alpha}{\pi\xi^2} + \alpha^2} \right\} . \end{aligned} \quad (15)$$

We see that the right hand side contains two exponentially decreasing terms. Provided both are positive, the right hand side of equation 15 will clearly be a decreasing function of q for all $q \geq 0$. The second term is positive since all of its factors are positive by definition. Now, by hypothesis, relation 15 is an equality for $q = 0$, so that the first term in 15 will also be positive provided that the second is $< 1/2$ for $q = 0$. This yields a quadratic constraint on α :

$$\alpha^2 - \frac{\alpha}{\pi\xi^2} + \frac{1}{4\pi\xi^2} > \left[\frac{k}{6\pi g\sigma_I\xi^2} \right]^2 \quad (16)$$

This now becomes our sufficient condition for inequality 15 to be fulfilled for all q .

Turning our attention to $S_0 > 0$, we observe by inspecting 14 that \mathcal{L} is an increasing function of S_0 for any fixed q provided only that

$$\alpha^2 - \frac{\alpha}{\pi\xi^2} + \frac{1}{6\pi\xi^2} > 0 \quad . \quad (17)$$

Thus, if we can find a value of α that simultaneously fulfills relation 14 as an equality, and fulfills inequalities 16 and 17, we have a convolution kernel that will allow rejection of cosmic rays without any excess risk of rejecting a valid pixel just because it contains flux from an object. In the next section, we determine the parameter space over which this is possible.

2.3. The choice of α

We now turn to deriving the value of α that fulfills our earlier assertion, satisfying 14 as an equality for $S_0 = 0$ and $q = 0$. This is easier if we first define the auxiliary parameter $\beta = 1/2 - \alpha$. The intuitive significance of β is that the expected counts in the filtered image J are $S_J(0) = \beta S_0$ at the location of a star having S_0 counts in original image I . Substituting $1/2 - \beta$ for α , setting S_0 and q to zero, and requiring exact equality, expression 14 becomes

$$\beta = \frac{k}{2g\sigma_I} \frac{\left(1 - \frac{1}{\pi\xi^2}\right) \left(\frac{1}{4} - \beta\right) + \beta^2 - \frac{1}{12\pi\xi^2}}{\sqrt{\left(1 - \frac{1}{\pi\xi^2}\right) \left(\frac{1}{4} - \beta\right) + \beta^2}} \quad . \quad (18)$$

This equation can be rearranged into a quartic in β (or equivalently α). Rather than doing so, we note that the present version can be solved iteratively for β by calculating the right hand side a few times, inserting $\beta = 0.25$ (or indeed any number in $[0, 0.25]$) the first time and using the previous result at each successive iteration. β is effectively a function of two parameters, $k/(g\sigma_I)$ and ξ . Now, for most imaging CCD data, we expect reasonable choices of these parameters to be $3 \lesssim k \lesssim 5$, $1 \lesssim g \lesssim 10$, $\sigma_I \gg 5/g$, and $\xi \gtrsim 1$ pixel. (Our estimate for σ_I is based on the assumption that the read noise is $\gtrsim 5$ electrons and the observer will typically ensure that sky noise is greater than read noise.) This leads to $k/(g\sigma_I) \ll 1$ under typical circumstances. In this limit, we expect

$$\beta \approx \beta_{\text{lim}} = \frac{1}{2} \left(\frac{k}{g\sigma_I} \right) \frac{1/4 - 1/(3\pi\xi^2)}{1/4 - 1/(4\pi\xi^2)} \quad . \quad (19)$$

One can further show that $\beta > \beta_{\text{lim}}$ under then nearly generic conditions that $0 \leq \beta < 1/4$ and $\beta < 1/2 - 1/(2\pi\xi^2)$. We therefore have a choice when implementing the algorithm between assuming $\beta = \beta_{\text{lim}}$ or solving equation 18 iteratively.

We have not derived analytically the range of parameter space over which β can be found iteratively, but empirically, the iterative solution will converge to a sensible result (fulfilling conditions 14, 16, and 17) provided that $0 < k/(g\sigma_I) < 2$ and that $\xi > 2/\sqrt{3\pi}$. These are our final set of sufficient conditions for this algorithm to work as desired. They are not as rigorously derived as conditions 14, 16, and 17, but do provide a quick check on when the method is likely to be applicable. Figure 2 shows contours of β as a function of ξ and $k/(g\sigma_I)$.

Given our formula for β , it is now also possible to determine $-C_J\sigma_I/(C_I\sigma_J)$ (the multiplicative reduction in significance level of a cosmic ray after convolution) as a function of ξ and $k/(g\sigma_I)$. Figure 3 shows contours of this efficiency factor.

3. Practical Implementation

We have implemented this algorithm and applied it to several data sets during the past year. In doing so, we introduced several enhancements of the basic algorithm that allow the method to run gracefully on our real data. Two particular artifacts were addressed by these enhancements. First, some bad pixels in some CCD cameras give data values far below the sky level B_I . If left alone, such pixels will cause many of their neighbors to be flagged as cosmic rays, since the wings of the convolution kernel will spread a strongly negative pixel in image I over many neighboring pixels in image J . Second, cosmic ray hits are often multiple-pixel events. In this case, a cosmic ray pixel may shield less strongly contaminated neighboring cosmic ray pixels from identification. An additional complication is that the background may not be spatially uniform, which hinders measuring the noise level in an image and defining a sensible threshold level for cosmic ray rejection.

The problems of low pixel values and spatially variable background levels can both be handled with preprocessing steps applied prior to the spatial convolution. Nonuniform sky level can be removed by generating and subtracting a smoothed map of the background intensity. I have chosen to use a large spatial median filter for this background generation, but any method working on larger spatial scales than the largest object in the frame would work. The main caveat is that a spatially constant rejection threshold should not be used if the background varies enough to introduce substantial spatial variations in the local Poisson sky noise. Low pixels can be flagged and replaced before the spatial convolution, using a simple threshold operation. This is of course best done after any variable background is subtracted, since the sky level should be uniform for the thresholding operation to be well behaved. Any previously known bad pixels can also be replaced with the background level or an interpolation from their good neighbors at this stage. This approach to background estimation has yielded good results for our data, in which large scale

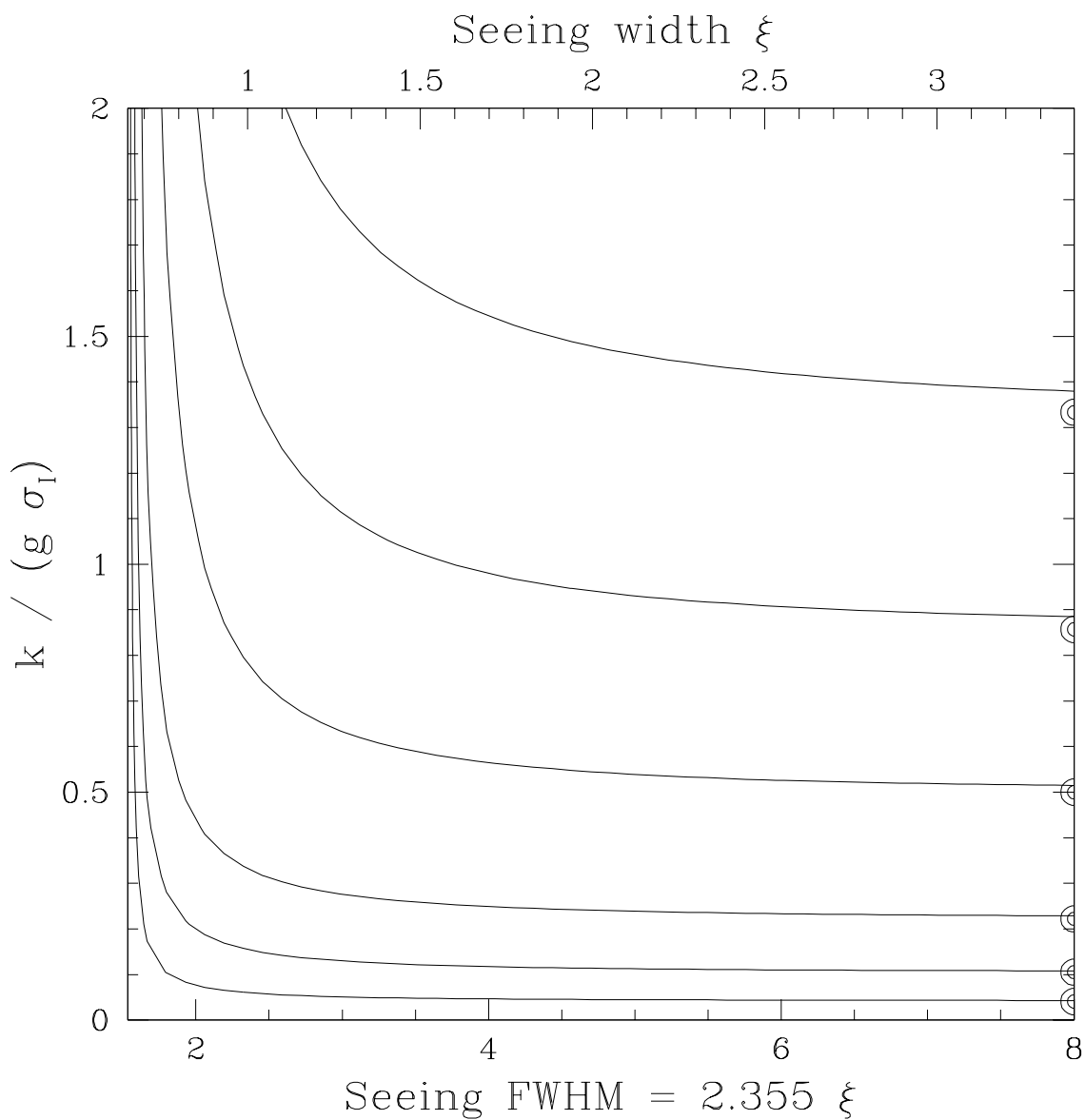


Fig. 2.— Contours show the optimal choice of $\beta = 1/2 - \alpha$ as a function of seeing ξ and the rejection threshold to noise ratio $k/(g\sigma_I)$. Contour levels (from top to bottom) are 0.20, 0.15, 0.10, 0.05, 0.025, and 0.01. Concentric semicircles at the right hand edge show the asymptotic value of $k/(g\sigma_I)$ for each contour curve in the limit $\xi \rightarrow \infty$.

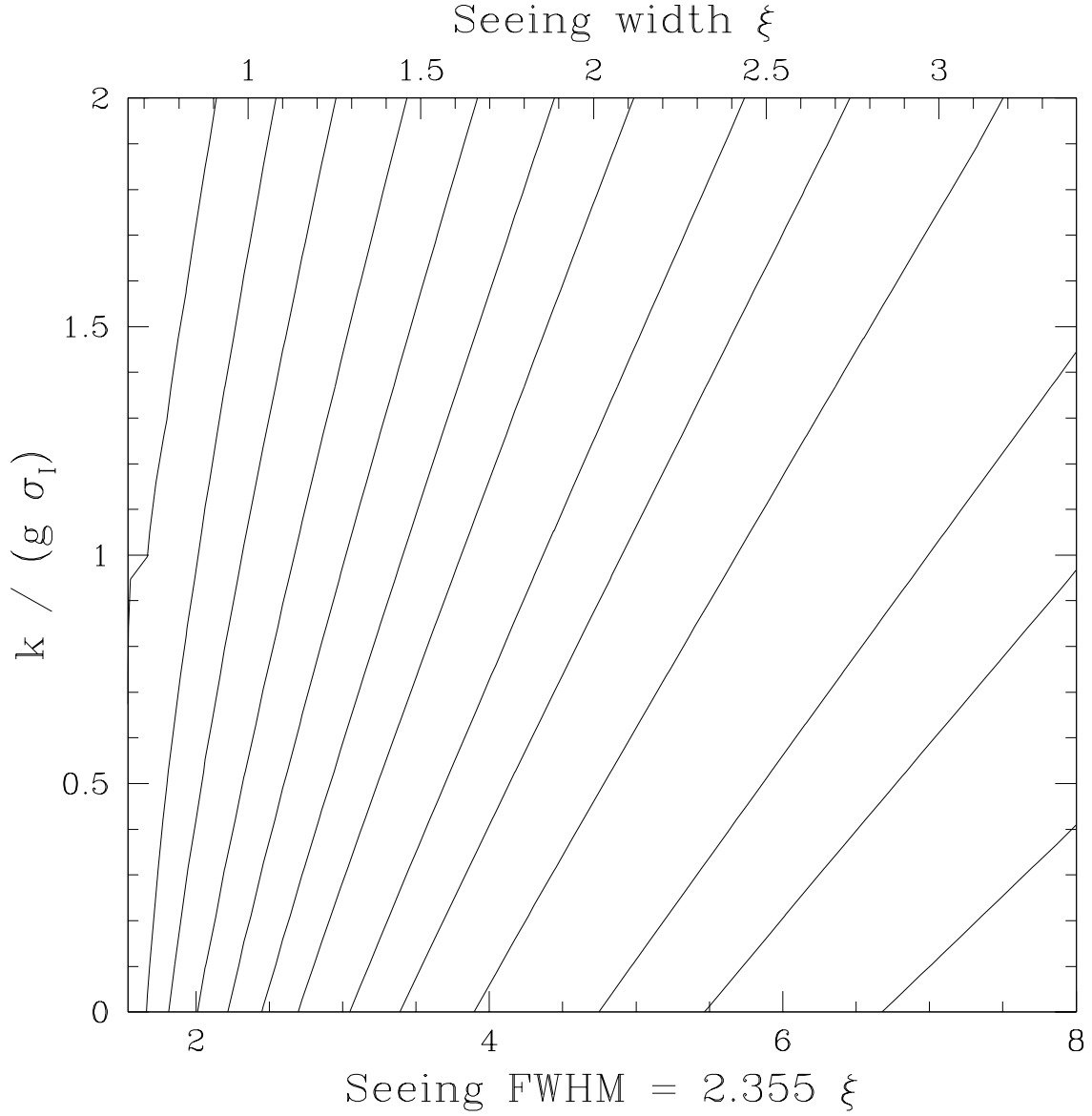


Fig. 3.— Contours show the factor $-C_J\sigma_I/(C_I\sigma_J)$ as a function of seeing ξ and the rejection threshold to noise ratio $k/(g\sigma_I)$, assuming that the optimal choice of β is used for the convolution kernel. Contour levels (starting at lower right) are 0.98, 0.97, 0.96, 0.94, 0.92, 0.90, 0.87, 0.84, 0.80, 0.75, 0.68, 0.60, and 0.50.

intensity variations are weak ($< 10\%$ of B_I) and due primarily to flatfielding errors. For cases where the intensity level contains structure on a wide range of spatial scales, multiscale transform methods (Starck, Murtagh, & Bijaoui 1995) can provide a natural treatment of the background level.

We estimate the variance in the input image empirically, using the iteratively clipped sample variance of the background-subtracted image to determine σ_I , which is taken to be spatially uniform. Spatial variations in the noise level could become a problem for some images. Such variations can be handled with a minor modification to the algorithm, by making the rejection threshold in the filtered image depend on the locally measured noise, provided only that the noise level variations occur on spatial scales large compared to the convolution kernel. Multiscale methods can again be used for accurate noise estimation in the presence of spatially variable backgrounds or extended objects (Starck & Murtagh 1998).

Some multiple-pixel cosmic ray hits will be well handled by a single convolution and flagging step, provided that they remain smaller than the PSF and that they are sufficiently strong (with intensities substantially exceeding the threshold for single pixel events). However, multiple-pixel events usually contain pixels with a range of intensities. When two contaminated pixels of very different intensity lie side by side, the stronger pixel will be flagged but the weaker one will be “shielded” from detection by its prominent neighbor. To identify such “shielded” cosmic ray pixels, the convolution and flagging algorithm can be run iteratively. After every flagging iteration, the newly identified cosmic ray pixels are replaced with the sky level, thereby exposing their less prominent neighbors to scrutiny. This iterative approach is highly successful at flagging all parts of a multi-pixel cosmic ray hit lying above the requested detection threshold.

When setting threshold levels for rejection, we have chosen to use empirical measures of the sky variance in both input and convolved image for convenience. Comparing the results of these empirical measures to the predicted relation given by equation 2 gave agreement at the 5–7% level for a test case with 3 pixel FWHM seeing (i.e., $\xi = 1.27$), with the measured variance of the convolved image slightly exceeding the prediction. Disagreements at this level could be due to several expected effects, e.g., the influence of real objects on the pixel histogram (which increases after smoothing), or the continuous approximation to discrete sums made in deriving equation 2.

This iterative cosmic ray rejection is of course computationally expensive when compared to basic image reduction steps like bias subtraction and flatfielding. Presently, eight iterations of cosmic ray rejection for a 2048×4096 pixel image requires of order 10 minutes to run on a 295 MHz Sun Ultra-30 with 248 megabytes of main memory. This speed could be improved by implementing the algorithm entirely in a compiled programming language (the present implementation being an interpreted IRAF script). It is nevertheless fast enough that I have routinely applied the algorithm to large data sets (tens of $2048 \times 4096 \times 8$ pixel images from the Kitt Peak National Observatory CCD Mosaic camera). In principle, the computational requirements should scale as $n \log(n)$ for n pixels in the large- n limit, since the convolution can be implemented using fast Fourier transforms,

while the remaining steps should all be linear in the number of pixels. Timing tests on a 400 MHz Intel Pentium-II computer with 128 megabytes of memory yielded a scaling of approximately $n^{1.4}$ for images with $\log_2(n) = 22 \pm 1$ (i.e. roughly 2k by 2k pixels). The difference between this scaling and the $n \log(n)$ scaling suggested from first principles is perhaps due to the variety of different computational demands (memory, i/o, cpu speed) which can limit the performance of the algorithm for different image sizes.

4. Simulations

To verify the analytical results of section 2 and study the effectiveness of the iterated algorithm on multiple pixel events, we carried out three types of artificial data simulations. The first type tested the algorithm’s detection rate for single pixel events; the second tested the false alarm rate at the locations of point sources; and the third tested rejection of multi-pixel events. For both tests of detection rates, the empirically measured detection threshold was taken as the intensity of added cosmic rays for which 50% of the affected pixels were correctly flagged. This is the appropriate cutoff because a simulated cosmic ray of precisely threshold intensity will be boosted above the cutoff by Poisson noise half the time, and will fall below threshold the other half.

The cosmic ray detection rate test added single pixel cosmic ray hits to a noise field and counted the number of hits correctly flagged by the algorithm as a function of CR intensity, rejection threshold, and PSF width. This allows a check of the analytic results plotted in figure 3. The agreement is good, with empirically measured detection thresholds falling between 100% and 110% of the theoretical expectations throughout the tested parameter space. In particular, the measured detection threshold is within 3% of the predicted value for $k/(g\sigma_I) \lesssim 0.3$, which is the regime of greatest interest for broadband astronomical imaging.

An interesting variant on the detection test is to run it on a field with stars or other astronomical objects. Our tests showed an appreciable degradation ($\sim 7\%$) of the CR detection threshold averaged over the image in the presence of a reasonably dense star field. This is expected, since the detection efficiency decreases in the wings of a point source (see section 2). However, there is no good way to characterize this effect for all possible images. If a precise measurement of the detection threshold in some particular image is needed, it can be obtained through simulations by adding “cosmic ray hits” to that exact image and studying their recovery rates.

The false alarm rate test examined the probability of rejecting a given pixel in a pure Poisson noise field with and without point sources. Only the central pixels of the point source locations were considered, since the wings of stellar profiles are less likely than their cores to be incorrectly rejected. This test confirmed that the probability of rejecting the central pixel of a star does not exceed the probability of rejecting an arbitrary sky pixel under our algorithm.

Finally, the multiple pixel event tests placed artificial bad columns onto noise fields and

measured the fraction of rejected pixels. Bad columns were chosen as a suitably conservative limiting case of multiple-pixel cosmic ray events, since such events usually have a linear morphology. The realized rejection threshold was determined as a function of stellar FWHM, number of adjacent bad columns, and requested sigma clipping level. These simulations were run with a sky noise of 41 ADU and gain of 3, so that they are restricted to low values of $k/(g\sigma_I)$. The general result is (unsurprisingly) that features comparable in size to the PSF cannot be rejected, while features much smaller than the PSF on only one axis can be rejected with relatively modest increases in the intensity threshold for rejection. Results of the multi-pixel event simulations are summarized in table 1.

5. Summary and Discussion

We have presented a cosmic ray rejection algorithm based on a convolution of the input image. The advantages of the method spring from the linear nature of the spatial filter, which allows us to determine the noise properties of the filtered image and so to calculate and control the probability of rejecting the central pixel (or indeed any pixel) of a point source. This safety mechanism ensures that cosmic ray rejection can be applied throughout the image, without special treatment for the locations of sources. The sensitivity to cosmic rays is of course reduced at the locations of objects, because of the added Poisson noise contributed by object photons and the resulting need to maintain a positive expectation value in the filtered image.

We usually apply our method conservatively, considering pixels innocent until proven guilty beyond any reasonable doubt. This means that given some uncertainty in the measured point spread function, we use a convolution kernel that is slightly narrower than our best estimate of the PSF (generally by about 10%). This choice depends on the relative importance of keeping legitimate sources and rejecting spurious ones for the scientific problem at hand.

Our original goal in developing this algorithm was to flag and replace cosmic ray hits in individual exposures that are later aligned and stacked. The alignment procedure requires interpolating the original images, and we use sinc interpolation to preserve the spatial resolution and noise properties of the input image. However, sinc interpolation assumes well sampled data and responds badly to cosmic rays, spreading their effects over many more pixels than were originally affected and motivating us to replace them at an early stage. We nevertheless have a second chance to reject cosmic rays by looking for consistency among our different exposures when we stack them, and this second chance helps motivate our generally conservative approach to cosmic ray flagging.

By applying the algorithm developed here followed by sigma rejection during image stacking, we exploit two distinct properties of cosmic rays: They are sharper than the point spread function, and they do not repeat from exposure to exposure. However, we are using these two tests in sequence. An algorithm exploiting both pieces of information simultaneously could potentially

yield more sensitive cosmic ray rejection. For general data sets, such an algorithm would have to handle stacks of unregistered images with different PSFs, making its development difficult but potentially rewarding. An interesting effort in this regard is Freudling's (1995) algorithm, which identifies cosmic rays in the course of deconvolving and coadding images with Hook & Lucy's (1992) method.

This work was supported by a Kitt Peak Postdoctoral Fellowship and by an STScI Institute Fellowship. Kitt Peak National Observatory is part of the National Optical Astronomy Observatories, operated by the Association of Universities for Research in Astronomy (AURA) under cooperative agreement with the National Science Foundation. The Space Telescope Science Institute (STScI) is operated by AURA under NASA contract NAS 5-26555. I thank an anonymous referee for their remarks.

REFERENCES

- Fischer, P. & Kochanski, G. P. 1994, *AJ* 107, 802
- Freudling, W. 1995, *PASP* 107, 85
- Hook, R. & Lucy, L. B. 1992, *ST-ECF Newslett.*, 17, 10
- Kendall, M. G., & Stuart, A. 1967, *The Advanced Theory of Statistics*, vol. 2, 2nd edition, New York: Hafner
- Murtagh, F. D. 1992, *ADASS* 1, 265
- Murtagh, F., & Adorf, H. M. 1991, *3rd ESO/ST-ECF Data Analysis Workshop*, P. Grosbol *et al*, eds., 51
- Salzberg, S., Chandar, R., Ford, H., Murthy, S. K., & White, R. 1995, *PASP* 107, 279
- Shaw, R. A., & Horne, K. 1992, *ADASS* 1, 311
- Starck, J.-L., Murtagh, F., & Bijaoui, A. 1995, *ADASS* 4, 279
- Starck, J.-L., & Murtagh, F. 1998, *PASP* 110, 193
- Windhorst, R. A., Franklin, B. E., & Neuschaefter, L. W. 1994, *PASP* 106, 798

Sigma cutoff	N_{cols}	Stellar FWHM							
		2	2.52	3.175	4	5.04	6.35	8	
3	1	0.34	0.57	0.74	0.80	0.86	0.90	0.94	
	2	0	0	0	0.40	0.56	0.70	0.80	
	3	0	0	0	0	0.19	0.39	0.58	
	4	0	0	0	0	0	0.12	0.31	
4	1	0.22	0.53	0.67	0.76	0.82	0.86	0.90	
	2	0	0	0	0.32	0.49	0.59	0.70	
	3	0	0	0	0	0.09	0.32	0.38	
	4	0	0	0	0	0	0.07	0.25	
5	1	0.16	0.52	0.63	0.73	0.81	0.85	0.89	
	2	0	0	0	0.23	0.43	0.50	0.63	
	3	0	0	0	0	0.06	0.27	0.36	
	4	0	0	0	0	0	0.04	0.21	

Table 1: The reduction in cosmic ray detection sensitivity for multiple pixel events consisting of adjacent bad columns of uniform value. The ratio of theoretical single pixel CR detection threshold to empirically determined multiple pixel threshold level is tabulated as a function of sigma cutoff, transverse size of the defect in columns, and point spread function width.